




Tunneling spectroscopic signatures of charge doping and associated Mott transition in α -RuCl₃ in proximity to graphite


Xiaohu Zheng ^{1,2,*}, Ke Jia ³, Junhai Ren,¹ Chongli Yang,¹ Xingjun Wu,¹ Youguo Shi,³ Katsumi Tanigaki,¹ and Rui-Rui Du ^{2,4}

¹Beijing Academy of Quantum Information Sciences, Beijing 100193, China

²International Center for Quantum Materials, School of Physics, Peking University, Beijing 100871, China

³Beijing National Laboratory for Condensed Matter Physics and Institute of Physics, Chinese Academy of Sciences, Beijing 100190, People's Republic of China

⁴CAS Center for Excellence in Topological Quantum Computation, University of Chinese Academy of Sciences, Beijing 100190, China

 (Received 2 May 2022; revised 27 March 2023; accepted 20 April 2023; published 5 May 2023)

The layered Mott insulator α -RuCl₃ has been extensively studied as a potential Kitaev quantum spin liquid candidate. Here, by constructing heterostructures with graphite, we employed electron tunneling measurements on few-layer α -RuCl₃ using scanning tunneling microscopy/spectroscopy. Characteristic tunneling spectra were detected on α -RuCl₃ layers in proximity to graphite. In the single-layer α -RuCl₃ in direct contact with graphite, distinct states in the Mott gap regime were observed. The in-gap states are demonstrated to be closely related to the electron orbitals in α -RuCl₃ and graphite, and to be sensitive to interfacial coupling, where a hybridization at the heterointerface is hypothesized. The in-gap states are also thought of as a charge reservoir for weakly doping the α -RuCl₃ upper layers. It demonstrated that the weak doping effect causes a considerable decrease in the Mott gap within the upper layers, suggesting that an unconventional Mott transition is occurring in these layers. The results show that the heterostructure comprising α -RuCl₃ and graphite is a good platform for investigating the doping physics in α -RuCl₃. Therefore, tunneling into such a doped system is a useful probe for studying otherwise insulating spin liquid candidates.

DOI: [10.1103/PhysRevB.107.195107](https://doi.org/10.1103/PhysRevB.107.195107)

I. INTRODUCTION

Kitaev quantum spin liquid (QSL) is a theoretical model of a strongly correlated spin phase. Its exact solution predicts the presence of Majorana zero mode (MZM) that obeys non-Abelian statistics, which could pave the way for fault-tolerant quantum computation [1,2]. A layered Mott insulator, α -RuCl₃ has been extensively investigated as a possible candidate for Kitaev QSL [3–8]. The fingerprints for Majorana fermions of the fractionalized spin excitations in α -RuCl₃ have been reported by several experimental groups [9–11]. Recent measurements of thermal Hall conductance with half-integer quantization, in particular, have provided important evidence for the chiral edge modes of Majorana fermions [12–20]. On the other hand, the roadmap designed for quantum technology platforms typically relies on electronic methods to manipulate the quantum bits [21]. The chargeless character of quasiparticles and the electrically insulating nature of Kitaev QSL materials like α -RuCl₃ would limit a range of suitable electronic measuring techniques. Recently, several experiment setups in heterostructures comprising conducting or superconducting films [22–31] have been proposed to exhibit electronic accessible signs of the quantum excitations in Kitaev QSL. Additionally, the doped Kitaev models are also

thought to host a number of exotic quantum phases, such as p -wave superconductivity [32–34], making charge doping in Kitaev QSL research more appealing and essential. On the experimental side, several groups have reported the charge doping of Kitaev materials via forming heterostructures with graphene [35–38], or ionic intercalations [39], but the doping mechanism of the Mott-insulating Kitaev honeycomb lattice remains elusive.

In this research, we transferred Kitaev QSL candidate material α -RuCl₃ flakes onto a highly oriented pyrolytic graphite substrate to create heterostructures, as illustrated schematically in Fig. 1(a). The surface morphology and electronic local density of states (LDOS) of α -RuCl₃ were evaluated by electron tunneling through the thin film using scanning tunneling microscopy and spectroscopy (STM/STS) after annealing the samples at 280°C in an ultrahigh-vacuum chamber for 2 h. We have attempted tunneling experiments on samples thicker than 20 nm; however, STM/STS can only be conducted at room temperature on those flakes. Thus, the samples in this study are all below 20 nm. The lock-in technique was used to measure STS at a frequency of 707 Hz and modulation amplitudes ranging from 5 to 8 mV. On dI/dV spectra, distinct states in the Mott gap regime were observed in the first α -RuCl₃ layer that directly contacts to graphite. It is demonstrated that the in-gap states result from orbital hybridization at the heterointerface. Surprisingly, a few upper layers exhibit a completely different spectral phenomenology than the bulk

*zhengxh@baqis.ac.cn

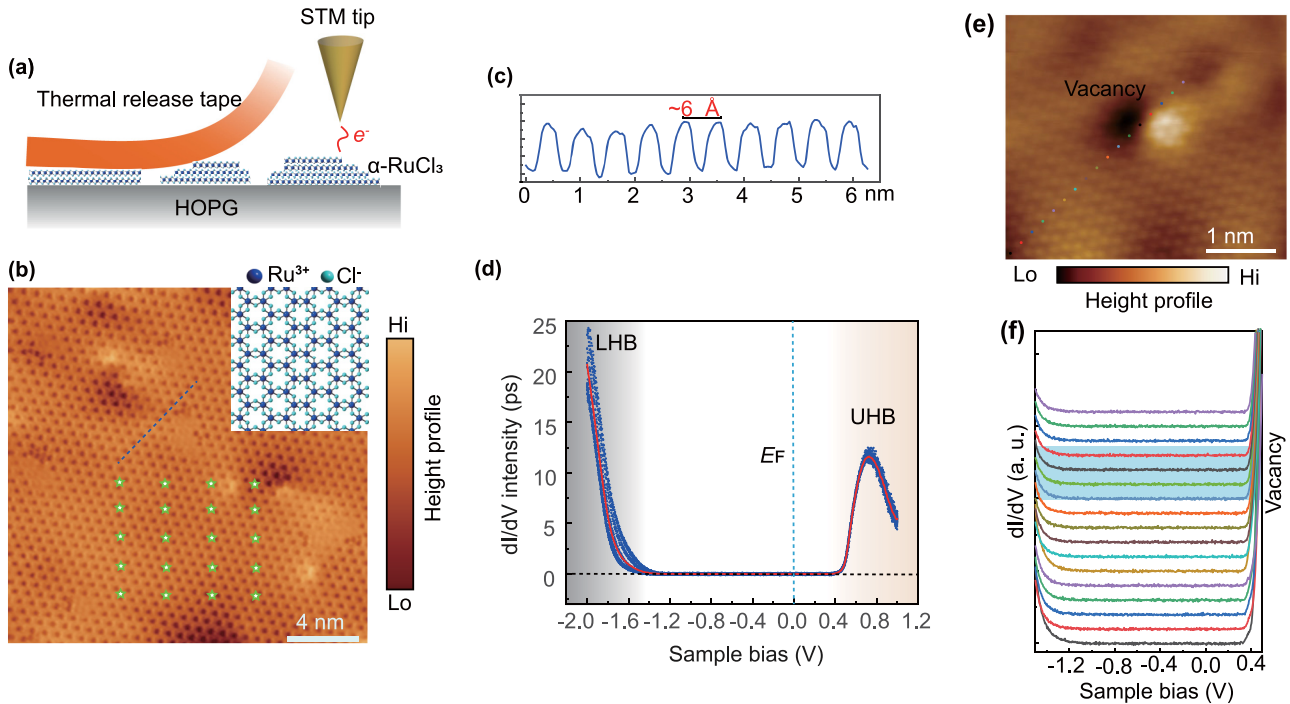


FIG. 1. (a) Schematic diagram of the experimental setup where the α - RuCl_3 flakes with different thicknesses are transferred by thermal release tap and measured through electron tunneling by STM/STS. (b) STM morphology of the bulk α - RuCl_3 (thickness >5 nm): The lattice constructions are presented in the inset (sample voltage: $V_H = 800$ mV; setpoint current: $I_s = 0.6$ nA). (c) Cross-sectional profile along the blue line shows the lattice constant is about 6 \AA . (d) dI/dV spectra taken at different locations (labeled with stars) on the surface in (b) (dark-blue curves) and an averaged dI/dV spectrum (red) show a full band gap of about 1.8 ± 0.2 eV ($V_H = 800$ mV, $I_s = 0.6$ nA). Colored shadow regions show the Hubbard bands. (e) STM morphology shows a single vacancy on α - RuCl_3 flake ($V_H = 550$ mV, $I_s = 1$ nA). (f) dI/dV spectral curves were collected at the locations as labeled by the corresponding colored dots in (e); spectra taken near the vacancy (shadowed with light blue) show negligible difference without any featured DOS arising in the Mott-gap regime ($V_H = 550$ mV, $I_s = 1$ nA).

α - RuCl_3 due to weak charge transfer from the heterointerface, where the Mott gap is significantly reduced. It implies that doping charges and strong quantum fluctuation in α - RuCl_3 combine to form a correlated insulating state with a reduced energy gap.

II. RESULTS AND DISCUSSION

α - RuCl_3 is an insulating $4d$ transition-metal halide with a honeycomb lattice composed of nearly ideal edge-sharing RuCl_6 octahedra [40,41]. Its basic structure is similar to that of graphite, where the bulk crystal can be exfoliated into a fully two-dimensional (2D) magnet, and the Ru atoms surrounded by Cl atoms form the 2D honeycomb lattice, as shown inset in Fig. 1(b). The amplitude and characteristics of the band gap, however, remain debatable; for example, the gap amplitude has been reported to range from 0.2 to 1.9 eV depending on the methodologies used [7,8,42,43]. In Fig. 1(b), an atomic-resolved STM morphology was taken on an α - RuCl_3 flake with a thickness more than 5 nm, which shows intrinsic properties of the bulk α - RuCl_3 . A honeycomb lattice with several vacancies were observed in Fig. 1(b). The lattice constant is approximately 6 \AA [Fig. 1(c)], which is consistent with the theoretical prediction [41]. The averaged dI/dV spectrum measured at 77 K, which is far above the Néel temperature ($T_N \sim 7 \text{ K}$) [11], reveals a U-shaped band gap of ~ 1.8 eV throughout the entire field of view [Fig. 1(d)].

In our experiment, the spectra are fully gapped without any single-particle excitations in the gap regime [Fig. 1(d)], and scarcely affected by disorders [Figs. 1(e) and 1(f)], showing a clear divergence from the spectrum taken at room temperature [42]. It coincides with the consensus that bulk α - RuCl_3 is a spin-orbital assisted Mott insulator in paramagnet phase [3], with significant Kitaev spin correlations that persist over a temperature range of 7 to 120 K [11,44–46]. Thus, in the spectra in Fig. 1(d), conduction- and valence bands with sharp edges correspond to the upper and lower Hubbard bands (UHB and LHB). The amplitude of the Mott gap is consistent with optically probed values [7], and calculations using the local-density approximation [7,47]. Overall, our tunneling experimental results on thick α - RuCl_3 flakes measured at 77 K have clearly highlighted the strong correlations and the Mott insulating natures of the bulk α - RuCl_3 [8,43].

As described in Refs. [32–35,48], charge transfer occurs when the heterostructure is made between α - RuCl_3 and graphene. The doping mechanism and electronic states of the weakly doped α - RuCl_3 are, however, still unclear. Here, in the samples of α - RuCl_3 on graphite, we focused on the thin α - RuCl_3 flakes that were in proximity to graphite. As shown in Fig. 2(a), a boundary region containing α - RuCl_3 terraces of single-layer (denoted as 1: α - RuCl_3) and bilayer (2: α - RuCl_3) on graphite was acquired with a broad-view STM image. The height profile of single-layer and bilayer α - RuCl_3 is approximately 600 pm [upper panel in Fig. 2(b)], which

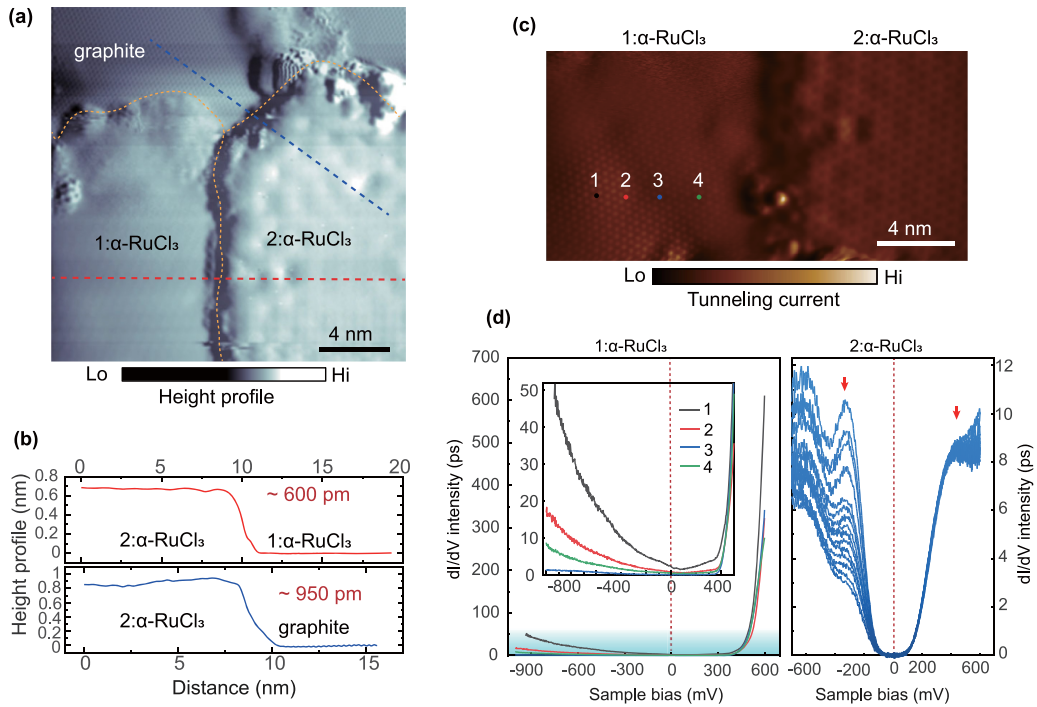


FIG. 2. (a) Broad-view STM image of the graphite surface covered by α - RuCl_3 flake with single and bilayer terraces (denoted as 1: α - RuCl_3 and 2: α - RuCl_3) ($V_H = 800$ mV; $I_s = 200$ pA). (b) Step profiles acquired between 2: α - RuCl_3 and 1: α - RuCl_3 ; 2: α - RuCl_3 and graphite, respectively. (c) High-resolution STM image across 1: α - RuCl_3 and 2: α - RuCl_3 ($V_H = 500$ mV; $I_s = 500$ pA). (d) Left: spatial dI/dV curves taken at numbered positions in (c) of the 1: α - RuCl_3 show the in-gap states are arising and the variations of spectra at different locations; enlarged view of the shadow regime is shown inset. Right: series of dI/dV spectra taken on the surface of the 2: α - RuCl_3 show the uniform reduced-gap spectral curves with a fluctuation of the occupied states ($V_H = 500$ mV, $I_s = 0.5$ nA).

is consistent with the anticipated thickness of single-layer α - RuCl_3 in van der Waals interlayer coupling [5,49]. We note that the thickness of monolayer α - RuCl_3 on graphite is only 350 pm, which is significantly less than the predicted value [5,49]. Despite the possibility of errors caused by the huge DOS difference (insulating vs metallic) on the neighboring sides, the interfacial coupling between graphite and α - RuCl_3 may be stronger than the general van der Waals due to probable interfacial hybridization. As demonstrated in Fig. 2(c), atomic-resolved STM images were employed on terraces of 1: α - RuCl_3 and 2: α - RuCl_3 , respectively. Spatial dI/dV spectra were collected in labeled positions on 1: α - RuCl_3 . Despite the fact that all the tunneling curves mimic the Mottness spectra with a large gap, as depicted in the left panel in Fig. 2(d), in-gap states were observed in an extended view of the gap regime [inset in Fig. 2(d)]. The in-gap states show spatially inhomogeneous intensities as moving tip positions, as shown inset in Fig. 2(d). The dI/dV spectra on the terrace of 2: α - RuCl_3 have a completely different line shape than those taken on the thick α - RuCl_3 and the single-layer flakes, and are uniform over the entire surface, where the energy gap is commonly and substantially reduced (~ 150 meV), as shown in the right panel of Fig. 2(d). The tunneling signatures in Fig. 2(d) indicate that considerable modifications of the electronic states are occurring in the first and second α - RuCl_3 layers on graphite.

We postulate that the modifications of α - RuCl_3 's electronic structures are caused by the heterostructures with graphite.

As a result, the first layer that directly contacts graphite is critical for understanding the underlying physics. As shown in the atomic-resolved STM images taken on the first α - RuCl_3 layer in Fig. 3(a), regions with mild lattice distortion are commonly observed due to the inhomogeneous coupling between α - RuCl_3 and graphite (artificially created by the transfer process). The appearance of the graphitelike lattice in the distortion zone [Fig. 3(a)] is fascinating. We carefully monitored a succession of tunneling spectra along the route, as shown in Fig. 3(a) (No. 1 to No. 10) under fixed tunneling parameters. When the positions are wide apart, the spectra exhibit U-shaped Mott gaps [from No. 1 to No. 4 in Fig. 3(b)], which are analogous to those on bulk α - RuCl_3 [Fig. 3(b)]. When the tip reaches the distortion [No. 5 to No. 10 in Fig. 3(b)] a broad in-gap state above the LHB arises and extends toward the E_F with a small peak developed at ~ -600 meV. There is essentially no change in the number of empty states along the path. The spectral phenomenology described above shows that hole puddles arise at the distortion regions on the surface of the first α - RuCl_3 layer. It explains the spatially inhomogeneous LDOS seen in Fig. 2(d), left.

What about the condition outside the distortion regime if the hole puddles are a consequence of the hybridization at the heterointerface? We discovered that the tunneling spectra are affected by the tunneling parameters, specifically the bias voltage V_H . As illustrated in Fig. 3(c), two representative sites, labeled No. 1 and No. 7, are chosen for measuring the dI/dV spectra under different tunneling conditions.

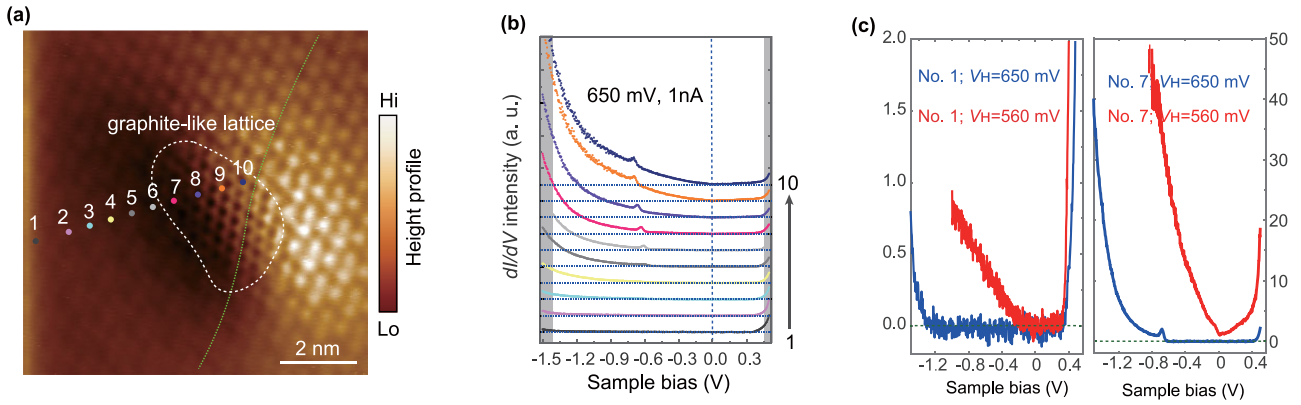


FIG. 3. (a) Atomic-resolved STM images are taken on 1: α -RuCl₃ ($V_H = 600$ mV; $I_s = 1$ nA); distortion of the lattice along the dashed green line can be seen, and the center of distortion (round with a dashed white line) presents a graphitelike lattice. (b) dI/dV spectra corresponding to the positions marked by colored dots (No. 1 to No. 10) in (a) show a clear evolution of LDOS. ($V_H = 650$ mV, $I_s = 1$ nA). (c) Comparison of dI/dV spectra collected at fixed positions No. 1 (left panel) and No. 7 (right panel) as labeled in (a) at different tunneling conditions by changing V_H from 650 to 560 mV with a fixed $I_s = 1$ nA.

Figure 3(c) shows dramatically improved in-gap states when V_H decreases from 650 to 560 mV in Fig. 3(c), where the gapped spectra practically turn to gapless. Such a huge variance in tunneling spectra cannot be interpreted by tip-induced band bending [50,51]. It implies that in-gap states exist even outside of the puddles on the α -RuCl₃ single layer. As a result, we hypothesize that hybridization commonly occurs at the heterointerface.

To further comprehend the tunneling signal as the setup parameters (V_H) varied, atomic-resolved STM images were taken in a fixed area [Fig. 4(a)] on 1: α -RuCl₃ with varying V_H . When $V_H = 800$ mV and $I_s = 600$ pA, the lattice of α -RuCl₃ is clearly visible across the entire region, as shown in Fig. 4(b). When V_H is reduced to 600 mV, a tiny distortion regime (DOS puddle) surrounded by α -RuCl₃ lattice forms in STM morphology, displaying the graphitelike lattice [Fig. 4(c)], acting similarly to that shown in Fig. 3(a). As V_H is decreased with a fixed I_s , the graphitelike lattice continually expands, eventually presenting on the entire area of the in view [from Figs. 4(d) to 4(g)]. It demonstrates the fact that hybridization occurs throughout the heterointerface, but the intensity of the hybridized states is tightly related to the interface coupling. As a result, the in-gap states in the region without distortion are faint and observable in low V_H (small tip-surface distance). We validated that the lattice constant and orientation of the graphitelike lattices are entirely consistent with the underneath graphite, as shown in Fig. 4(a). As is generally known, STM morphology is a convolution of the scanned surface's topography and electronic states. When the electronic wave functions (EWFs) from the beneath layer successfully dominate the tunneling current, the underneath topographic signals can be disclosed on top of heterostructures [52]. Even at a low sample voltage [$V_H = 410$ mV in Fig. 4(g)], the associated energy remains outside the Mott gap on 1: α -RuCl₃ (in UHB). It suggests that at the heterointerface, overlapping charge orbitals from both α -RuCl₃ and graphite layers contributed to the tunneling signals on the surface, resulting in the graphitelike lattice architecture.

We took the dI/dV spectra at the locations indicated by the stars in Fig. 4(d) with different tunneling parameters to observe the LDOS corresponding to the STM topographic evolution. In Fig. 4(h), left, we see that decreasing V_H with a fixed I_s results in a peaked DOS at ~ -1350 meV above the LHB at $V_H < 550$ mV. We started to witness the graphitelike lattice emerging in the selected point in Fig. 4(e) in an approximate V_H , indicating that the distinct in-gap state accounts for the emergence of graphitelike lattice on α -RuCl₃ surface. However, by comparing the in-gap states to the DOS in the dI/dV spectrum of bare graphite, the hypothesis that the peaked states originate solely from the underlying graphite may be ruled out, as shown in right panel in Fig. 4(h). It also implies that the peaked states are caused by the heterointerfacial hybridization. As V_H decreases, the in-gap state arises quickly above LHB and extends to E_F . Another minor LDOS peak at -600 meV, shown in Fig. 3(b), reappears in Fig. 4(h), left, with $V_H = 450$ mV. As V_H decreases further, the peaked LDOS at -600 meV submerges into the fast-increasing in-gap states. At this point, the spectrum is substantially equal to the spectrum shown in the right panel in Fig. 3(c) (red curve), suggesting that the LDOS outside of the lattice distortion are nearly identical to those in the distortion region within the decreased V_H . On the other hand, while the gap can be completely closed with finite state at E_F at $V_H < 450$ mV, both the UHB and LHB are still conserved in a broadly viewed energy scale [Fig. 4(h)], indicating that the hybridization did not collapse the Mott-Hubbard state.

We performed the following study to get compelling proof that the in-gap states are caused by heterointerfacial hybridization rather than tip-surface interactions. The tunneling parameters V_H and I_s were used to position the STM tip on the surface at a specific distance d_s [inset in Fig. 4(i)], and the spectra were acquired by sweeping the sample bias (V_b) while suspending the feedback loop. d_s can be quantitatively calculated using the formula $d_s = -\frac{\hbar}{2\sqrt{2m\Phi}} \ln\left(\frac{R_0 I_s}{V_H}\right)$, where m is the mass of the tunneling electron, Φ is the average work function of the tip and the sample, and R_0 is the resistance for

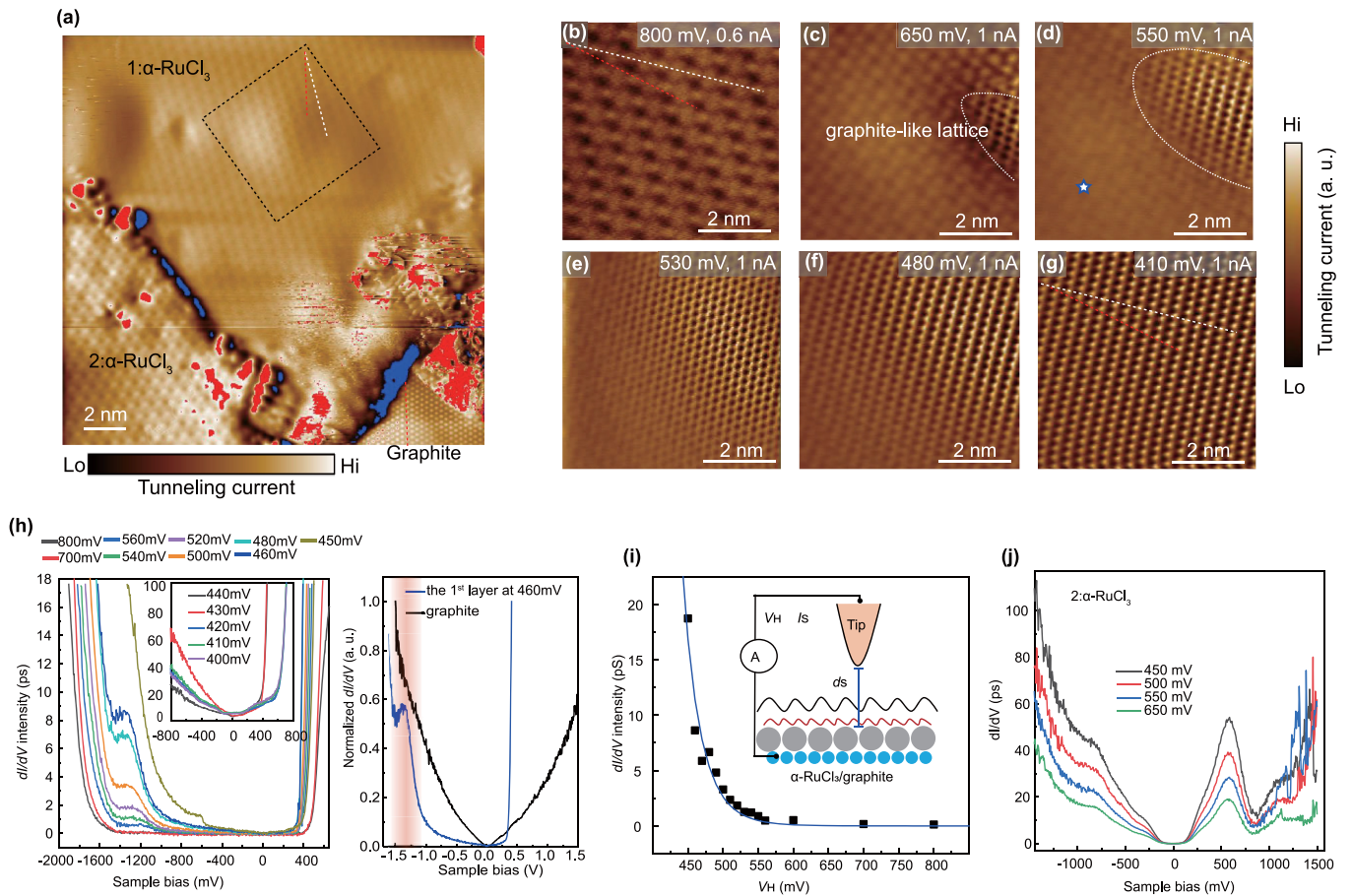


FIG. 4. (a) Broad-view STM image (tunneling current channel) shows lattice topographies of the single-layer (1: α - RuCl_3), bilayer α - RuCl_3 (2: α - RuCl_3), and graphene substrate. Lattice orientations in the three regions can be distinguished, where the white and red dashed lines represent the lattice orientations of 1: α - RuCl_3 and graphite, respectively. (b)–(g) STM morphologies taken on 1: α - RuCl_3 with variation of tunneling conditions show evolution from α - RuCl_3 to the graphite-like lattice, the evolution begins at the region with slight lattice distortion. (h) Left: dI/dV spectra on 1: α - RuCl_3 acquired with changing V_H from 800 to 400 mV with a fixed $I_s = 1$ nA; in-gap states peaked at -1350 meV arising in the Mott gap; Right: normalized dI/dV spectrum taken on the first α - RuCl_3 layer with $V_H = 460$ mV and $I_s = 1$ nA, is compared to the normalized spectrum taken on a bare graphite ($V_H = 1$ V and $I_s = 0.5$ nA). (i) Peak magnitude at -1350 meV as a function of V_H is fitted using the distance-dependent Tersoff and Hamann tunneling formalism [54]. Inset schematically shows the experimental setup when dI/dV was performed, where the orbitals can be selectively detected by tuning V_H ; j) dI/dV spectra were taken on the 2: α - RuCl_3 with variation of V_H with a fixed $I_s = 1$ nA.

a single-atomic point contact [53]. The Tersoff and Hamann tunneling formalism [54] can thus be used to explain dI/dV spectra associated with d_s : $\frac{dI}{dV} \propto e^{-2kd_s} N(eU_{\text{bias}})$, where k is a constant, and $N(eU_{\text{bias}})$ is the surface LDOS at a certain bias voltage U_{bias} . dI/dV spectra would be tunable by modulating the work function (Φ) of the tip or introducing the tip-surface interactions (R_0), such as the spreading resistance effect [51] and the tip-induced band bending [50]. Indeed, the tip-surface interactions increase DOS amplitude and shift band edges in the dI/dV spectra on α - RuCl_3 flakes with different thicknesses [Figs. 4(h) and 4(j)], but they never introduce distinct characteristics (peaked DOS) to the spectra curves. By making the parameters related to the tip and tip-surface interaction constant, the tip-dominated states can be avoided. As a result, only true surface states can be well fitted using the Tersoff and Hamann formalism [54]. In Fig. 4(i), we fit the data using the distinct state that peaked at -1350 meV. The growing tendency of peak amplitude over V_H fits nicely,

proving that the in-gap states truly existed. However, as shown schematically in Fig. 4(i), they have a short decay length. The results in Fig. 4 demonstrated that EWFs from both layers overlap, resulting in the formation of an occupied subband that peaked at -1350 meV above the LHB.

An intriguing question arises: May charges from the in-gap states at the heterointerface be transferred to the upper α - RuCl_3 layers? Is the doping effect, if so, a precursor to a new electronic phase? The completely distinct dI/dV spectra on the second α - RuCl_3 layer [on the right of Fig. 2(d)] appear promising. As a result, the tunneling spectra on few-layer α - RuCl_3 must be investigated. Figure 5(a) shows a different α - RuCl_3 flake on graphite. The surfaces of the terraces in the square [designated in Fig. 5(a)] are the third and the fourth α - RuCl_3 layers above the graphite [left panel of Fig. 5(c)], is illustrated by a height profile [Fig. 5(b)] along the dashed line in Fig. 5(a). Unlike the bulk morphology of the bulk α - RuCl_3 where the honeycombs are constructed by Ru atoms as seen

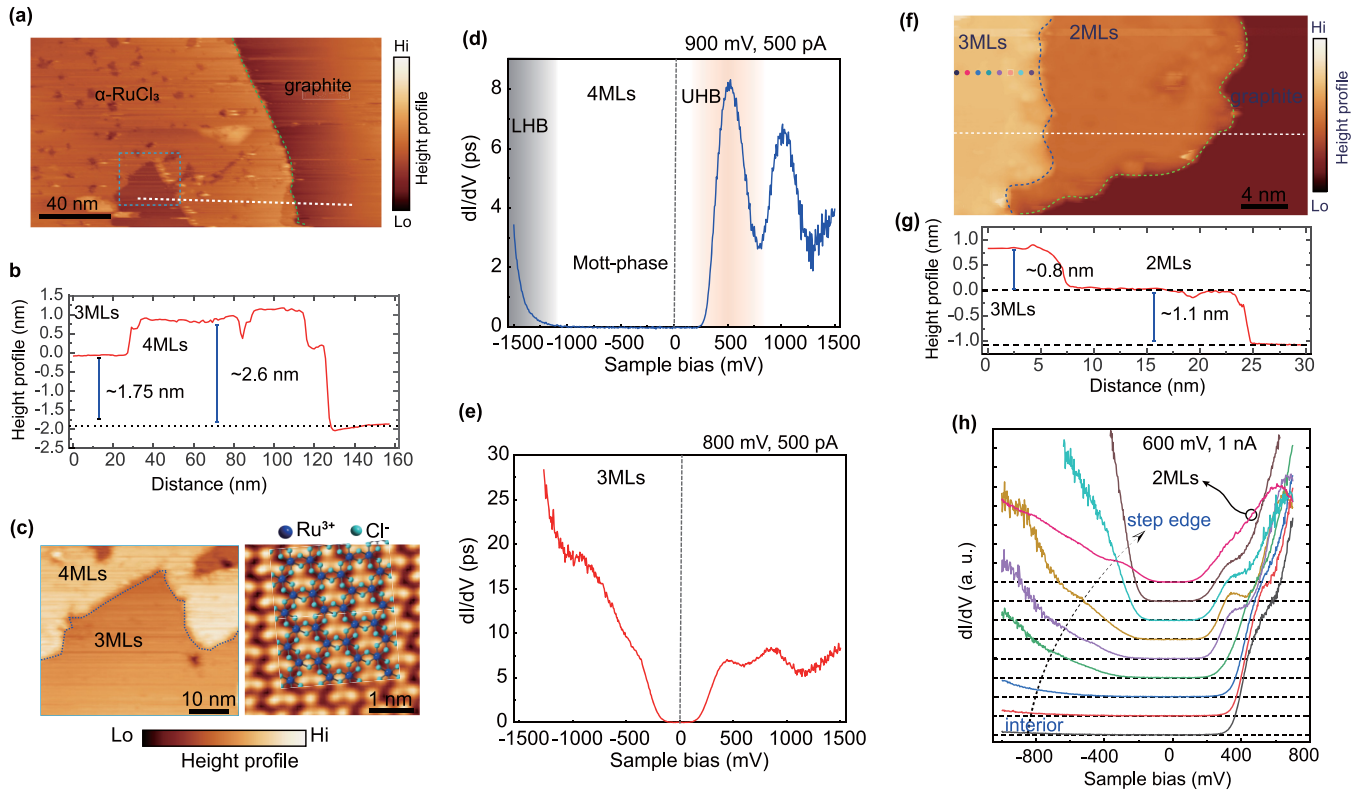


FIG. 5. (a) Broad-view STM image of α -RuCl₃ terraces on graphite ($V_H = 1$ V; $I_s = 500$ pA). (b) Height profile along the dashed white line shows the thicknesses of the α -RuCl₃ terraces in the squared region correspond to surfaces of the third and fourth layers, respectively. (c) Left: an enlarged STM image of the third and fourth α -RuCl₃ terraces ($V_H = 1$ V; $I_s = 500$ pA); Right: atomic-resolved STM topography on the third layer filtered by reversed Fourier transform reveals the sites of Cl atoms. (d), (e) Averaged dI/dV spectra acquired on the fourth ($V_H = 900$ mV, $I_s = 500$ pA) and third ($V_H = 800$ mV, $I_s = 500$ pA) layers, respectively. Two representative spectra show the possible Mott-phase transition between the fourth and third layers. (f) STM morphology shows another α -RuCl₃ flake on graphite ($V_H = 600$ mV; $I_s = 1$ nA). (g) Height profile along the dashed white line in (f) shows the thicknesses correspond to the surfaces of the third and second α -RuCl₃ layers on graphite. (h) dI/dV spectra are collected precisely at each colored point as marked on the third layer in (f) near the step edge, with an averaged dI/dV spectrum taken on the second layer for comparison ($V_H = 600$ mV, $I_s = 1$ nA).

in Fig. 1(b), the STM image on the third layer reveals a lattice structure dominated by the Cl atoms, as shown in the right panel of Fig. 5(c). It means that the surface electronic states of the third layer have changed dramatically. As illustrated in Figs. 5(d) and 5(e), averaged dI/dV spectra are taken on the two terrace surfaces (the third and the fourth layers, respectively). The fourth layer retains a U-shaped spectral curve (>1.4 eV) similar to the spectra on the bulk α -RuCl₃, whereas the third layer has a spectrum with a suppressed gap (~ 330 meV) qualitatively similar to the spectra on the second layer in Fig. 1(d).

Figure 5(f) shows another flake-containing surfaces of the second and third α -RuCl₃ layers. Because of the inhomogeneous interface coupling in different flakes, the surfaces of the second layer has a thickness of ~ 1.1 nm (Fig. 5(g)), which is slightly thicker than that in Fig. 2(b). The reduced-gap spectra were observed on the second layer [Fig. 5(h)] in this region, confirming a common characteristic of the second layer above graphite. However, the gap amplitude (~ 250 meV) is larger than that in Fig. 2(b) (~ 170 meV), as is the thickness (1.1 vs 0.95 nm). The third layer exhibits a U-shaped Mott gap far away from the step (interior of the

terrace), while the dI/dV spectra reveal a crossover from the large U-shaped Mott gap to the reduced gap as the tip approaches the step edge [Fig. 5(h)]. The crossover process is dominated by the elevation of occupied states and filling holes in the Mott gap, demonstrating the tight relationship to the in-gap states in the first layer. With the emergence of a subband near 300 meV, the UHB transfers its spectral weight to the low-energy side. When we compared the thicknesses of the third α -RuCl₃ layers in different flakes in Figs. 5(b) and 5(g), we discovered that the thickness in Fig. 5(g) (~ 1.9 nm) is also slightly larger than that in Fig. 5(b) (~ 1.75 nm), indicating that the thickness, i.e., the interface coupling, is more important than the layer number for the possible Mott transition. The above results show that the possible Mott transition is caused by charge doping from the heterointerface rather than being a layer-dependent phenomenon. The possible Mott transition typically happens in the second and third layers, where the charges from the heterointerface can be transferred. Angle-resolved photoemission spectroscopy [8] and optoelectronic measurement [39] previously discovered similar Mott transitions in charge-doped α -RuCl₃, where the Mott gap is similarly suddenly lowered upon ionic doping. It was thought

to be caused by the relationship between doping charges and significant spin fluctuation [8]. We still do not fully comprehend the possible unconventional Mott transition in this work. The mechanism of the possible unconventional Mott transition merits more investigation.

III. CONCLUSION

In conclusion, distinct states were detected in the Mott gap in α -RuCl₃ single layer that is directly contacted to graphite; huge modulations of the tunneling spectra with transferring Hubbard bands to low-energy sides and a dramatically reduced Mott gap were observed on the upper-layer α -RuCl₃ (generally on surfaces of the second and third layers); and the crossover from the large-gapped Mott insulator to the insulator with reduced gap was observed at the step edge in an α -RuCl₃ flake. Based on the experiment results, we propose that the overlap of EWFs between graphite and α -RuCl₃ at the heterointerface causes in-gap states in the first α -RuCl₃ layer, and then the charges from the heterointerface are transferred

into the upper layers to induce a weak doping and a possible unconventional Mott transition of α -RuCl₃. The findings show an intriguing electronic phenomenon in the doped α -RuCl₃ Kitaev QSL system, which warrants future theoretical and experimental exploration.

ACKNOWLEDGMENTS

We would like to thank Deepak Karki for helpful discussion. This work was supported by National Basic Research & Development plan of China (Grant No. 2019YFA0308400), the National Natural Science Foundation of China (Grant No. U2032204), and the Strategic Priority Research Program of the Chinese Academy of Sciences (Grants No. XDB28000000 and No. XDB33030000).

X.H.Z. and J.H.R. fabricated heterostructure samples; X.H.Z. conducted the STM experiments; K.J., C.L.Y., and Y.G.S. provided the α -RuCl₃ samples; X.H.Z. analyzed the data; X.H.Z., X.J.W., K.T., and R.-R.D. wrote the paper; X.H.Z. and R.-R.D. conceived the project; and all authors contributed to discussions of the results.

-
- [1] A. Kitaev, Anyons in an exactly solved model and beyond, *Ann. Phys.* **321**, 2 (2006).
- [2] A. Yu. Kitaev, Fault-tolerant quantum computation by anyons, *Ann. Phys.* **303**, 2 (2003).
- [3] K. W. Plumb, J. P. Clancy, L. J. Sandilands, V. V. Shankar, Y. F. Hu, K. S. Burch, H.-Y. Kee, and Y.-J. Kim, α -RuCl₃: A spin-orbit assisted mott insulator on a honeycomb lattice, *Phys. Rev. B* **90**, 041112(R) (2014).
- [4] Y. Kubota, H. Tanaka, T. Ono, Y. Narumi, and K. Kindo, Successive magnetic phase transitions in α -RuCl₃: XY-like frustrated magnet on the honeycomb lattice, *Phys. Rev. B* **91**, 094422 (2015).
- [5] H. B. Cao, A. Banerjee, J. Q. Yan, C. A. Bridges, M. D. Lumsden, D. G. Mandrus, D. A. Tennant, B. C. Chakoumakos, and S. E. Nagler, Low-temperature crystal and magnetic structure of α -RuCl₃, *Phys. Rev. B* **93**, 134423 (2016).
- [6] A. Koitzsch, C. Habenicht, E. Müller, M. Knupfer, B. Büchner, H. C. Kandpal, J. van den Brink, D. Nowak, A. Isaeva, and Th. Doert, J_{eff} Description of the Honeycomb Mott Insulator α -RuCl₃, *Phys. Rev. Lett.* **117**, 126403 (2016).
- [7] S. Sinn, C. H. Kim, B. H. Kim, K. D. Lee, C. J. Won, J. S. Oh, M. Han, Y. J. Chang, N. Hur, H. Sato *et al.*, Electronic structure of the Kitaev material α -RuCl₃ probed by photoemission and inverse photoemission spectroscopies, *Sci. Rep.* **6**, 39544 (2016).
- [8] X. Zhou, H. Li, J. A. Waugh, S. Parham, H.-S. Kim, J. A. Sears, A. Gomes, H.-Y. Kee, Y.-J. Kim, and D. S. Dessau, Angle-resolved photoemission study of the Kitaev candidate α -RuCl₃, *Phys. Rev. B* **94**, 161106(R) (2016).
- [9] S.-H. Baek, S.-H. Do, K.-Y. Choi, Y. S. Kwon, A. U. B. Wolter, S. Nishimoto, J. van den Brink, and B. Büchner, Evidence for a Field-Induced Quantum Spin Liquid in α -RuCl₃, *Phys. Rev. Lett.* **119**, 037201 (2017).
- [10] A. Banerjee, J. Yan, J. Knolle, C. A. Bridges, M. B. Stone, M. D. Lumsden, D. G. Mandrus, D. A. Tennant, R. Moessner, and S. E. Nagler, Neutron scattering in the proximate quantum spin liquid α -RuCl₃, *Science* **356**, 1055 (2017).
- [11] S.-H. Do, S.-Y. Park, J. Yoshitake, J. Nasu, Y. Motome, Y. S. Kwon, D. T. Adroja, D. J. Voneshen, K. Kim, T.-H. Jang *et al.*, Majorana fermions in the Kitaev quantum spin system α -RuCl₃, *Nat. Phys.* **13**, 1079 (2017).
- [12] Y. Kasahara, S. Suetsugu, T. Asaba, S. Kasahara, T. Shibauchi, N. Kurita, H. Tanaka, and Y. Matsuda, Quantized and unquantized thermal Hall conductance of Kitaev spin-liquid candidate α -RuCl₃, *Phys. Rev. B* **106**, L060410 (2022).
- [13] T. Yokoi, S. Ma, Y. Kasahara, S. Kasahara, T. Shibauchi, N. Kurita, H. Tanaka, J. Nasu, Y. Motome, C. Hickey *et al.*, Half-integer quantized anomalous thermal Hall effect in the Kitaev material candidate α -RuCl₃, *Science* **373**, 568 (2021).
- [14] Y. Kasahara, K. Sugii, T. Ohnishi, M. Shimozawa, M. Yamashita, N. Kurita, H. Tanaka, J. Nasu, Y. Motome, T. Shibauchi *et al.*, Unusual Thermal Hall Effect in a Kitaev Spin Liquid Candidate α RuCl₃, *Phys. Rev. Lett.* **120**, 217205 (2018).
- [15] Y. Kasahara, T. Ohnishi, Y. Mizukami, O. Tanaka, S. Ma, K. Sugii, N. Kurita, H. Tanaka, J. Nasu, Y. Motome *et al.*, Majorana quantization and half-integer thermal quantum Hall effect in a Kitaev spin liquid, *Nature (London)* **559**, 227 (2018).
- [16] P. Czajka, T. Gao, M. Hirschberger, P. Lampen-Kelley, A. Banerjee, J. Yan, D. G. Mandrus, S. E. Nagler, and N. P. Ong, Oscillations of the thermal conductivity in the spin-liquid state of α -RuCl₃, *Nat. Phys.* **17**, 915 (2021).
- [17] P. Czajka, T. Gao, M. Hirschberger, P. Lampen-Kelley, A. Banerjee, N. Quirk, D. G. Mandrus, S. E. Nagler, and N. P. Ong, Planar thermal Hall effect of topological bosons in the Kitaev magnet α -RuCl₃, *Nat. Mater.* **22**, 36 (2023).
- [18] J. Nasu, Thermal Transport in the Kitaev Model, *Phys. Rev. Lett.* **119**, 127204 (2017).
- [19] T. Minakawa, Y. Murakami, A. Koga, and J. Nasu, Majorana-Mediated Spin Transport in Kitaev Quantum Spin Liquids, *Phys. Rev. Lett.* **125**, 047204 (2020).

- [20] J. a. N. Bruin, R. R. Claus, Y. Matsumoto, N. Kurita, H. Tanaka, and H. Takagi, Robustness of the thermal Hall effect close to half-quantization in α -RuCl₃, *Nat. Phys.* **18**, 401 (2022).
- [21] D. Aasen, M. Hell, R. V. Mishmash, A. Higginbotham, J. Danon, M. Leijnse, T. S. Jespersen, J. A. Folk, C. M. Marcus, K. Flensberg *et al.*, Milestones Toward Majorana-Based Quantum Computing, *Phys. Rev. X* **6**, 031016 (2016).
- [22] G. Kishony and E. Berg, Converting electrons into emergent fermions at a superconductor–Kitaev spin liquid interface, *Phys. Rev. B* **104**, 235118 (2021).
- [23] M. G. Yamada and S. Fujimoto, Electric Probe for the Toric Code Phase in Kitaev Materials through the Hyperfine Interaction, *Phys. Rev. Lett.* **127**, 047201 (2021).
- [24] R. G. Pereira and R. Egger, Electrical Access to Ising Anyons in Kitaev Spin Liquids, *Phys. Rev. Lett.* **125**, 227202 (2020).
- [25] D. Aasen, R. S. K. Mong, B. M. Hunt, D. Mandrus, and J. Alicea, Electrical Probes of the Non-Abelian Spin Liquid in Kitaev Materials, *Phys. Rev. X* **10**, 031014 (2020).
- [26] S.-Q. Jia, L.-J. Zou, Y.-M. Quan, X.-L. Yu, and H.-Q. Lin, Electron tunneling spectroscopy of an anisotropic Kitaev quantum spin liquid sandwiched between superconductors, *Phys. Rev. Res.* **4**, 023251 (2022).
- [27] M. Udagawa, S. Takayoshi, and T. Oka, Scanning Tunneling Microscopy as a Single Majorana Detector of Kitaev’s Chiral Spin Liquid, *Phys. Rev. Lett.* **126**, 127201 (2021).
- [28] S. Biswas, Y. Li, S. M. Winter, J. Knolle, and R. Valentí, Electronic Properties of α -RuCl₃ in Proximity to Graphene, *Phys. Rev. Lett.* **123**, 237201 (2019).
- [29] J. Feldmeier, W. Natori, M. Knap, and J. Knolle, Local probes for charge-neutral edge states in two-dimensional quantum magnets, *Phys. Rev. B* **102**, 134423 (2020).
- [30] M. Carrega, I. J. Vera-Marun, and A. Principi, Tunneling spectroscopy as a probe of fractionalization in two-dimensional magnetic heterostructures, *Phys. Rev. B* **102**, 085412 (2020).
- [31] E. J. König, M. T. Randeria, and B. Jäck, Tunneling Spectroscopy of Quantum Spin Liquids, *Phys. Rev. Lett.* **125**, 267206 (2020).
- [32] U. F. P. Seifert, T. Meng, and M. Vojta, Fractionalized Fermi Liquids and Exotic Superconductivity in the Kitaev-Kondo Lattice, *Phys. Rev. B* **97**, 085118 (2018).
- [33] W. Choi, P. W. Klein, A. Rosch, and Y. B. Kim, Topological superconductivity in the Kondo-Kitaev model, *Phys. Rev. B* **98**, 155123 (2018).
- [34] V. S. de Carvalho, R. M. P. Teixeira, H. Freire, and E. Miranda, Odd-frequency pair density wave in the Kitaev-Kondo lattice model, *Phys. Rev. B* **103**, 174512 (2021).
- [35] B. Zhou, J. Balgley, P. Lampen-Kelley, J.-Q. Yan, D. G. Mandrus, and E. A. Henriksen, Evidence for charge transfer and proximate magnetism in graphene- α -RuCl₃ heterostructures, *Phys. Rev. B* **100**, 165426 (2019).
- [36] D. J. Rizzo, S. Shabani, B. S. Jessen, J. Zhang, A. S. McLeod, C. Rubio-Verdú, F. L. Ruta, M. Cothrine, J. Yan, D. G. Mandrus *et al.*, Nanometer-scale lateral p–n junctions in graphene/ α -RuCl₃ heterostructures, *Nano Lett.* **22**, 1946 (2022).
- [37] D. J. Rizzo, B. S. Jessen, Z. Sun, F. L. Ruta, J. Zhang, J.-Q. Yan, L. Xian, A. S. McLeod, M. E. Berkowitz, K. Watanabe *et al.*, Charge-transfer plasmon polaritons at graphene/ α -RuCl₃ interfaces, *Nano Lett.* **20**, 8438 (2020).
- [38] S. Mashhadi, Y. Kim, J. Kim, D. Weber, T. Taniguchi, K. Watanabe, N. Park, B. Lotsch, J. H. Smet, M. Burghard *et al.*, Spin-split band hybridization in graphene proximitized with α -RuCl₃ nanosheets, *Nano Lett.* **19**, 4659 (2019).
- [39] M. Jo, H. Heo, J.-H. Lee, S. Choi, A. Kim, H. B. Jeong, H. Y. Jeong, J. M. Yuk, D. Eom, J. Jahng *et al.*, Enhancement of photoresponse on narrow-bandgap Mott insulator α -RuCl₃ via intercalation, *ACS Nano* **15**, 18113 (2021).
- [40] I. Pollini, Electronic properties of the narrow-band material α -RuCl₃, *Phys. Rev. B* **53**, 12769 (1996).
- [41] H.-S. Kim and H.-Y. Kee, Crystal structure and magnetism in α -RuCl₃: An *ab initio* study, *Phys. Rev. B* **93**, 155143 (2016).
- [42] M. Ziatdinov, A. Banerjee, A. Maksov, T. Berlijn, W. Zhou, H. B. Cao, J.-Q. Yan, C. A. Bridges, D. G. Mandrus, S. E. Nagler *et al.*, Atomic-scale observation of structural and electronic orders in the layered compound α -RuCl₃, *Nat. Commun.* **7**, 13774 (2016).
- [43] L. J. Sandilands, Y. Tian, A. A. Reijnders, H.-S. Kim, K. W. Plumb, Y.-J. Kim, H.-Y. Kee, and K. S. Burch, Spin-orbit excitations and electronic structure of the putative Kitaev magnet α -RuCl₃, *Phys. Rev. B* **93**, 075144 (2016).
- [44] L. J. Sandilands, C. H. Sohn, H. J. Park, S. Y. Kim, K. W. Kim, J. A. Sears, Y.-J. Kim, and T. W. Noh, Optical probe of Heisenberg-Kitaev magnetism in α -RuCl₃, *Phys. Rev. B* **94**, 195156 (2016).
- [45] A. Koitzsch, E. Müller, M. Knupfer, B. Büchner, D. Nowak, A. Isaeva, T. Doert, M. Grüninger, S. Nishimoto, and J. van den Brink, Low-temperature enhancement of ferromagnetic Kitaev correlations in α -RuCl₃, *Phys. Rev. Mater.* **4**, 094408 (2020).
- [46] L. J. Sandilands, Y. Tian, K. W. Plumb, Y.-J. Kim, and K. S. Burch, Scattering Continuum and Possible Fractionalized Excitations in α -RuCl₃, *Phys. Rev. Lett.* **114**, 147201 (2015).
- [47] H. Y. Liu, Z. F. Hou, C. H. Hu, Y. Yang, and Z. Z. Zhu, Electronic and magnetic properties of fluorinated graphene with different coverage of fluorine, *J. Phys. Chem. C* **116**, 18193 (2012).
- [48] E. Gerber, Y. Yao, T. A. Arias, and E.-A. Kim, *Ab Initio* Mismatched Interface Theory of Graphene on α -RuCl₃: Doping and Magnetism, *Phys. Rev. Lett.* **124**, 106804 (2020).
- [49] R. D. Johnson, S. C. Williams, A. A. Haghighirad, J. Singleton, V. Zapf, P. Manuel, I. I. Mazin, Y. Li, H. O. Jeschke, R. Valentí *et al.*, Monoclinic crystal structure of α -RuCl₃ and the zigzag antiferromagnetic ground state, *Phys. Rev. B* **92**, 235119 (2015).
- [50] R. M. Feenstra, J. A. Stroscio, and A. P. Fein, Tunneling spectroscopy of the Si(111) 2×1 surface, *Surf. Sci.* **181**, 295 (1987).
- [51] V. Ramachandran and R. M. Feenstra, Scanning Tunneling Spectroscopy of Mott-Hubbard States on the 6H-SiC(0001) $\sqrt{3}\times\sqrt{3}$ Surface, *Phys. Rev. Lett.* **82**, 1000 (1999).
- [52] A. J. Fisher, Scanning Probe microscopy, theory, in *Encyclopedia of Spectroscopy and Spectrometry*, 3rd ed., edited by J. C. Lindon, G. E. Tranter, and D. W. Koppenaal (Academic Press, Oxford, 2017), pp. 23–28.
- [53] Y. Takahashi, T. Miyamachi, K. Ienaga, N. Kawamura, A. Ernst, and F. Komori, Orbital Selectivity in Scanning Tunneling Microscopy: Distance-Dependent Tunneling Process Observed in Iron Nitride, *Phys. Rev. Lett.* **116**, 056802 (2016).
- [54] J. Tersoff and D. R. Hamann, Theory and Application for the Scanning Tunneling Microscope, *Phys. Rev. Lett.* **50**, 1998 (1983).